Rotational degree-of-freedom synthesis: An optimised finite difference method for non-exact data

T.J. Gibbons [a,*], E. Öztürk [b], N.D. Sims [a]

[a] Department of Mechanical Engineering, The University of Sheffield, Mappin Street, Sheffield S1 3JD, United Kingdom
[b] Advanced Manufacturing Research Centre with Boeing, The University of Sheffield, Wallis Way, Catcliffe, Rotherham S60 5TZ, United Kingdom

A B S T R A C T

Measuring the rotational dynamic behaviour of a structure is important for many areas of dynamics such as passive vibration control, acoustics, and model updating. Specialist and dedicated equipment is often needed, unless the rotational degree-of-freedom is synthesised based upon translational data. However, this involves numerically differentiating the translational mode shapes to approximate the rotational modes, for example using a finite difference algorithm. A key challenge with this approach is choosing the measurement spacing between the data points, an issue which has often been overlooked in the published literature.

The present contribution will for the first time prove that the use of a finite difference approach can be unstable when using non-exact measured data and a small measurement spacing, for beam-like structures. Then, a generalised analytical error analysis is used to propose an optimised measurement spacing, which balances the numerical error of the finite difference equation with the propagation error from the perturbed data. The approach is demonstrated using both numerical and experimental investigations. It is shown that by obtaining a small number of test measurements it is possible to optimise the measurement accuracy, without any further assumptions on the boundary conditions of the structure.

© 2017 The Authors. Published by Elsevier Ltd. This is an open access article under the CC BY license (http://creativecommons.org/licenses/by/4.0/).

1. Introduction

Experimental rotational degrees-of-freedom (RDOF) are required in many areas of dynamics, such as structural modification [1,2], acoustics [3], and model updating/reduction [4,5]. Whilst the measurement of translational data is now commonplace, the same cannot be said for their rotational counterparts. Although techniques exist to directly measure RDOFs, they usually require specialist equipment, such as laser vibrometers or rotational accelerometers, which may not be readily available. For this reason, synthesis methods are often used to extract rotational information form translational data, which can be measured using standard test equipment. The most common is the finite difference (FD) technique, first proposed by Sattinger in 1978 [6].

The method applies a finite difference equation to data collected from closely spaced sensors to numerically differentiate the translational data with respect to the spatial coordinate. However, as with any numerical method, its accuracy is dependent on the choice of spacing between data points. It is well documented that the accuracy of a FD equation can be improved by reducing the spacing; this paper will show that when using non-exact measured data (data containing some error), the method becomes unstable. As the spacing is decreased, small errors or perturbations in the input data, such as noise or misalignment, give rise to

large errors in the output. Hence, a compromise must be found, which balances the numerical error of the FD equation with the perturbation propagation error from the data.

Whilst the numerical errors associated with finite difference equations are well known, little attention has been paid to the propagation error. For this reason the application of the FD method for rotational degree-of-freedom synthesis is not robust. In this paper, a full analytic error analysis of the FD method in the modal domain is carried out, showing that, for any structure, the method becomes unstable when using non-exact data. The results from the error analysis are used to propose an optimum spacing to balance the two errors. However, the optimum spacing relies on knowledge of two unknown quantities, the high order derivatives of the translational data and the error contained in the measurement. Analytical solutions for the mode shapes of beams are used to show that, for certain finite difference equations, this information can be found from the translational modal model, whilst for all other finite difference equations, a good approximation can also be found. An experimental investigation is also carried out to show how effective the method can be when approximating the measurement error.

The applications of experimentally derived rotational degrees-of-freedom are vast and varied. Schmitz et al. [1,2] proposed a structural modification method, called receptance coupling substructure analysis (RCSA), as a method to avoid chatter in machining operations such as milling. Moorhouse et al. [3] used the finite difference method in order to characterise structure-borne sound sources for use in assembled structures, such as vehicles and machinery. And the Craig-Brampton method [5] (more commonly known today as component mode synthesis) was originally proposed as a model reduction method. Whilst these applications are promising, they are all limited by the need for highly accurate information on the rotational degrees-of freedom. As stated above, this paper concentrates on the FD method, partly due to its simplicity, but also due to the lack of robust error analysis available for the method.

Sattinger first considered the problem of rotational degree-of-freedom synthesis in 1980 [6], showing that any rotational frequency response function (FRF) is equal to the spatial derivative of its translational equivalent. The finite difference method was then used to approximate such derivatives. Using a free-free beam as an example, it was found that the results were accurate close to resonance, whilst other areas of the FRF showed considerable scatter. Although it was shown (using theoretical data) that a smaller spacing increases the accuracy of the numerical method, the link between increasing the spacing and decreasing the scatter was not made. Sestieri et al. [7] also used the example of a free-free beam, this time with experimental data. They suggested an improvement in the result could be found by using a spacing of between 5% and 8% of the total beam length; however, they failed to recognise that the error level may vary between different experiments and with different beams.

Duarte and Ewins [8,9] later looked at the same problem and had similar issues, noting that the spacing of the accelerometers affects not only the scatter in the results but also the position of the antiresonances. The paper was also the first to apply the finite difference method in the modal domain. Again using data from a free-free beam, rotational mode shapes were approximated by applying the FD equation directly to the measured mode shapes, and then the rotational FRFs constructed from the result. This was found to give more accurate results than application in the frequency domain, but carried the added difficulty of how to include high frequency residuals. A high frequency pseudo mode was found to give satisfactory results. Although the paper suggests that the quality of the result is directly linked to the spacing, it is also concluded that the selection of the appropriate spacing remains a problem.

The only theoretical error analysis of the finite difference method for use in rotational DOF synthesis came from Elliot [10,11]. In this case, using a simply supported beam as an example, it was shown that the numerical error associated with FD equations is directly proportional to the spacing between the sensors. However, the paper does not go on to show that the perturbation propagation error is inversely proportional to the spacing; instead arguing that, due to improvements in measurement equipment/practice, this should be less of a problem.

2. Background

The translational displacement of a structure can be characterised by its mode shapes $\phi_r(x)$ and their corresponding eigenvalues ω_r^2, which are easily related to the frequency response function (FRF), H_{ij}, usually measured in modal testing.

$$H_{ij}(\omega) = \frac{Y_i(\omega)}{F_j(\omega)} = \sum_{r=1}^{N} \frac{\phi_r(x_i)\phi_r(x_j)}{\omega_r^2 - \omega^2} \tag{1}$$

Here, $H_{ij}(\omega)$ is the FRF excited at location i and measured at location j for a particular frequency ω, Y_i is the Fourier transform of the displacement at location i, F_j is the Fourier transform of the input force at location j, N is the total number of modes measured, $\phi_r(x_i)$ is the rth mode at location i, and the magnitude of ω_r is the rth natural frequency.

However, the above equation only makes up part of the full response model often required for the applications discussed in section 1, as it only considers the translational displacement, Y, and excitation force, F. To fully understand the vibration of any structure both rotational displacement Θ and excitation moment M must also be included, giving rise to three further FRFs:

$$N_{ij}(\omega) = \frac{\Theta_i}{F_j} = \sum_{r=1}^{N} \frac{\phi_r^{(1)}(x_i)\phi_r(x_j)}{\omega_r^2 - \omega^2} \qquad L_{ij}(\omega) = \frac{Y_i}{M_j} = \sum_{r=1}^{N} \frac{\phi_r(x_i)\phi_r^{(1)}(x_j)}{\omega_r^2 - \omega^2} \qquad P_{ij}(\omega) = \frac{\Theta_i}{M_j} = \sum_{r=1}^{N} \frac{\phi_r^{(1)}(x_i)\phi_r^{(1)}(x_j)}{\omega_r^2 - \omega^2} \tag{2}$$

Whilst the measurement of these FRFs is difficult, mainly due to the application of a pure moment, Eq. (2) shows that they can be constructed from the standard modal model (ϕ_r, ω_r) and the rotational mode shapes $\phi_r^{(1)}$ (where the superscript (1) represents
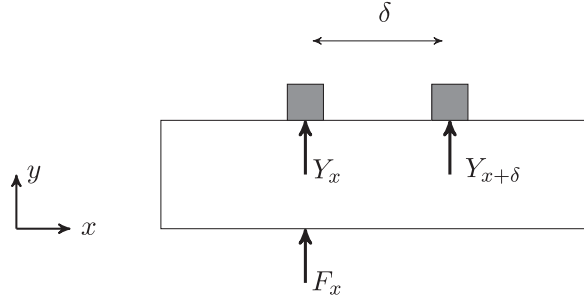
Fig. 1. Application of the first order forward finite difference equation in the modal domain.

the first derivative). Hence, by measuring the mode shapes and eigenvalues, and using this data to approximate the rotational mode shapes, it is possible to construct a full response model.

Perhaps the simplest method of approximating the derivative of a mode shape is the first order forward finite difference equation, a standard result derived from the truncated Taylor series. Defining the forward finite difference operator, D_δ^F, we have that:

$$\phi_r^{(1)}(x) \approx D_\delta^F \phi_r(x) = \frac{\phi_r(x + \delta) - \phi_r(x)}{\delta} \tag{3}$$

where x is the coordinate of interest on the structure, δ is a small length on the structure, and ϕ_r has a continuous bounded derivative. In application, the mode shape is measured using two sensors (separated by δ), as shown in Fig. 1, then Eq. (3) is used to approximate its derivative. It should be noted that it is not necessary for the co-located FRF to occur at the point of interest, and higher order finite difference equations can be also be applied using additional sensors.

2.1. Error analysis

By Taylor's theorem [12], provided ϕ_r has a continuous bounded second derivative ($\phi_r^{(2)}$) the truncation error of the above approximation (Eq. (3)) is bounded by:

$$\left| \phi_r^{(1)}(x) - D_\delta^F \phi_r(x) \right| \leq \frac{\delta}{2} \|\phi_r^{(2)}\| \tag{4}$$

where $\|\phi_r^{(2)}\|$ is the Euclidean norm of the vector $\phi_r^{(2)}$. This result is derived in Appendix A. The general form of such forward difference equations (for the first derivative) can be written as

$$D_\delta^F \phi_r(x) = \frac{1}{\delta} \sum_{k=0}^{n} a_k \phi_r(x + k\delta) \tag{5}$$

Here, $a_k \in \mathbb{R}$ are the coefficients found from the Taylor series derivation, and n is the number of additional nodes in the finite difference method. For the example given in Eq. (3), $a_k = \{-1, 1\}$, and $n = 1$. Similar to the above example, the general truncation error is given by

$$\left| \phi_r^{(1)}(x) - D_\delta^F \phi_r(x) \right| \leq T\delta^n \|\phi_r^{(n+1)}\| \tag{6}$$

where the specific truncation coefficient $T \in \mathbb{R}$ can be found by analysing the Taylor series truncation. For the example given in Eq. (4), $T = 1/2$.

This, however, is not the only error when using finite difference equations with measured data [13]. Consider the measured mode shape ϕ_{rm}, which is the sum of the actual mode shape ϕ_r and some measurement perturbation $\overline{\phi}_r$. Hence,

$$\phi_{rm} = \phi_r + \overline{\phi}_r \tag{7}$$

This perturbation may contain signal noise as well as measurement or curve fitting errors. When a finite difference equation is applied to such data, it is applied to both the mode shape and the perturbation, giving rise to the so called propagation error. Similar to the idea of the truncation error in Eq. (6), an upper bound on the propagation error must also be found. Consider any point x in the region of interest, then

$$|\phi_r(x) - \phi_{rm}(x)| \leq \|\phi_r - \phi_{rm}\| \leq M_r \tag{8}$$

Here, $\|\phi_r - \phi_{rm}\|$ is the Euclidean distance between the vectors ϕ_r and ϕ_{rm}, and M_r is defined as the upper bound on the measurement perturbation of the rth mode, i.e.

$$\|\overline{\phi}_r\| \leq M_r \tag{9}$$

Then, applying the above forward difference equation (Eq. (5)) to the perturbed data, we have that

$$
\begin{aligned}
D_\delta^F \phi_{rm}(x) &= \frac{1}{\delta} \sum_{k=0}^n a_k \phi_{rm}(x + k\delta) \\
&= \frac{1}{\delta} \left(\sum_{k=0}^n a_k \phi_r(x + k\delta) + \sum_{k=0}^n a_k \overline{\phi}_r(x + k\delta) \right) \\
&= D_\delta^F \phi_r(x) + \frac{1}{\delta} \sum_{k=0}^n a_k \overline{\phi}_r(x + k\delta)
\end{aligned}
\tag{10}
$$

Therefore, the noise propagation error can be bounded by:

$$
\left| D_\delta^F \phi_r(x) - D_\delta^F \phi_{rm}(x) \right| = \left| \frac{1}{\delta} \sum_{k=0}^n a_k \overline{\phi}_r(x + k\delta) \right| \leq \frac{M_r}{\delta} \sum_{k=0}^n |a_k|
\tag{11}
$$

Hence, by combining the truncation error in Eq. (6) with the noise propagation error in Eq. (11), a bound on the total error (e_T) is given by:

$$
e_T = \left| \phi_r^{(1)}(x) - D_\delta^F \phi_{rm}(x) \right| \leq \left| \phi_r^{(1)}(x) - D_\delta^F \phi_r(x) \right| + \left| D_\delta^F \phi_r(x) - D_\delta^F \phi_{rm}(x) \right| \leq T\delta^n \|\phi_r^{(n+1)}\| + \frac{M_r}{\delta} \sum_{k=0}^n |a_k|
\tag{12}
$$

Herein lies the most significant problem of the application of finite difference formulae with real data. As $\delta \to 0$ the truncation error tends to zero, whilst the propagation error tends to infinity and the method becomes unstable.

2.2. A new optimum spacing

By minimising the upper bound of the total error, the total error itself will be minimised; therefore, a value of δ must be chosen so as to balance the two terms and minimise the right hand side (RHS) of Eq. (12). This may be found by setting the first derivative (with respect to δ) of the RHS of Eq. (12) to zero, then the resultant δ_{min}^F is found to be:

$$
\delta_{min}^F = \left(\frac{M_r}{nT} \sum_{k=0}^n |a_k| \|\phi_r^{(n+1)}\|^{-1} \right)^{\frac{1}{n+1}}
\tag{13}
$$

Making the same assumptions on the continuity of ϕ_r as above, and following the same process, the optimum spacing for the general backward difference equations (δ_{min}^B) is found to be the same function. Whilst for central differences δ_{min}^C is given by:

$$
\delta_{min}^C = \left(\frac{M_r}{2nT} \sum_{k=-n}^n |a_k| \|\phi_r^{(2n+1)}\|^{-1} \right)^{\frac{1}{2n+1}}
\tag{14}
$$

Whilst it is advantageous to have an optimum spacing for each individual mode, for structures with many modes, it may become experimentally expensive to capture a separate dataset for each mode shape. In this case, each of the individual optimum spacings should be calculated and an average taken, such that:

$$
\begin{aligned}
\delta_{min}^F &= \sum_{r=0}^R \left(\frac{M_r}{nT} \sum_{k=0}^n |a_k| \|\phi_r^{(n+1)}\|^{-1} \right)^{\frac{1}{n+1}} \\
\delta_{min}^C &= \sum_{r=0}^R \left(\frac{M_r}{2nT} \sum_{k=-n}^n |a_k| \|\phi_r^{(2n+1)}\|^{-1} \right)^{\frac{1}{2n+1}}
\end{aligned}
\tag{15}
$$

Where R is the total number of modes considered. The effect of averaging the optimum spacings is discussed in section. 6.

The formulae and necessary coefficients (T, $\sum a_k$) for the forward, backward and central difference equations for $n = 1$, $n = 2$, and $n = 3$ are summarised in Tables B.1, B.2, and B.3 respectively. However, the optimum spacings given in Eqs. (13) and (14) still contain two unknown values, firstly, the high order derivative norm $\|\phi_r^{(p)}\|$ (where $p = n + 1$ for forward/backward differences, and $p = 2n + 1$ for central differences), and secondly, the measurement perturbation bound M_r.

The next two sections deal with how to evaluate the derivative norms $\|\phi_r^{(p)}\|$. A numerical investigation is used to validate the optimised measurement spacing when assuming perfect knowledge of the measurement perturbation bound M_r.

3. Evaluating the fourth order derivative norms

The aim of the section is to validate the new optimum spacings for the finite difference method with non-exact data. Numerical examples are used so that the measurement perturbation bound M_r can be calculated exactly, leaving the only unknown value as the high order derivative norm $\|\phi_r^{(p)}\|$. Using the analytical solutions for the mode shapes of beams with arbitrary boundary conditions, it will be shown that for forward/backward finite difference equations of order $n = 4k - 1$ where $k = 1, 2, 3, \ldots$, the exact value of $\|\phi_r^{(p)}\|$ can be calculated from the translational modal model (ϕ_r, ω_r).

3.1. The fourth derivative of beam mode shapes

The general form of the *rth* mode shape for an Euler-Bernoulli beam is given by:

$$\phi_r(x) = C_1 \cosh(\lambda_r x) + C_2 \sinh(\lambda_r x) + C_3 \cos(\lambda_r x) + C_4 \sin(\lambda_r x) \tag{16}$$

where constants C_1 to C_4 are found from the boundary conditions and

$$\lambda_r^4 = \frac{\rho A \omega_r^2}{EI} \tag{17}$$

where ρ is the material density, A is the cross-sectional area, E is the Young's modulus, and I is second moment of inertia.

Due to the inherent trigonometric/hyperbolic nature of such mode shapes, certain relationships between Eq. (16) and its higher order derivatives can be found. The trigonometric functions will repeat every fourth derivative, and the hyperbolic functions every second, therefore:

$$\phi_r^{(4)} = \lambda_r^4 \phi_r \tag{18}$$

Hence, when using the forward/backward difference equations and the optimum spacing given in Eq. (13), by choosing $n = 3$ the norm of the fourth derivative is required, meaning the finite difference equation can be optimised without any approximation. The optimum spacing then simplifies to

$$\delta_{min}^F = \frac{1}{\lambda_r} \left(\frac{80 M_r}{9 \|\phi_r\|} \right)^{\left(\frac{1}{4} \right)} \tag{19}$$

Following the same logic it is also possible to show that

$$\phi_r^{(4k)} = \lambda_r^{4k} \phi_r \quad \text{where} \quad k = 1, 2, 3, \ldots \tag{20}$$

meaning the exact value for d_{min}^F can be found for all finite differences of order $n = 4k - 1$.

3.2. A beam with arbitrary boundary conditions

Since no assumptions on the boundary conditions (BCs) of the beam were made, the above result may be applied to both beam and beam like structures. Hence for validation purposes, a finite element model of a 0.5 m cylindrical beam of diameter 0.01 m (shown in Fig. 2 section A) was constructed, and extended in both directions to give arbitrary BCs. One boundary (B1) was comprised of a 0.5 m square beam of 0.02 m width pinned at one end, whilst the other (B2) consisted of a 0.3 m cylindrical beam of diameter 0.02 m fixed at one end. The eigenvalue problem was solved over the whole beam and a normal mode model extracted across section A, which contained 501 equally spaced nodes. The response to an impulse, applied at boundary B1, with maximum amplitude of 1 N and time step of 1.25×10^{-5} s, was then simulated for each of the 501 nodes.
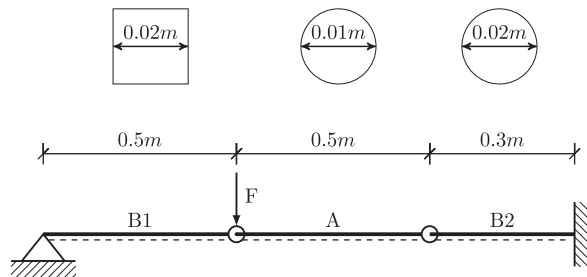

Fig. 2. The geometry and boundary conditions of a beam used for numerical validation of error analysis.
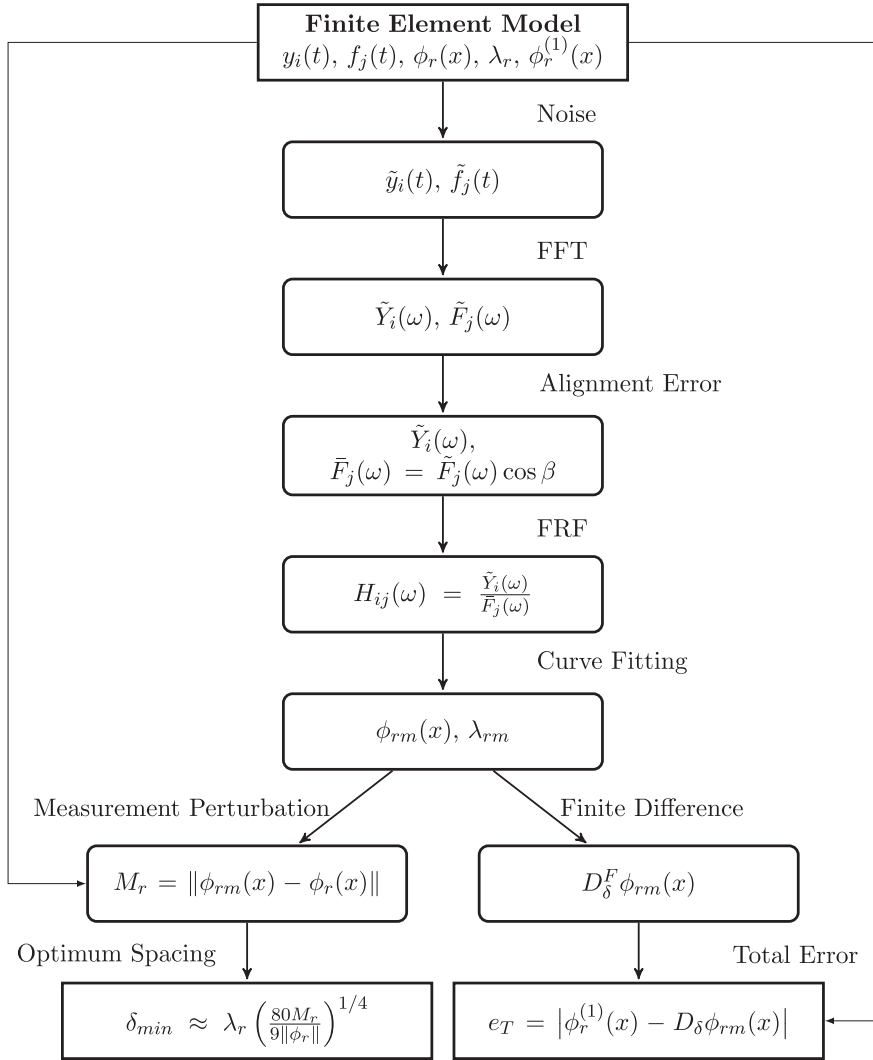
Fig. 3. Flow chart detailing the process followed to calculate optimum spacings δ_{min} (left hand side) in numerical investigation, and total error e_T (right hand side) for numerical validation of error analysis.

3.3. Numerical validation

Since noise and error in measurement is random and varies from test to test and from signal to signal, a statistical investigation is needed to validate the error analysis.

Firstly, using the result given in Eq. (19) the optimum spacings for the first 5 bending modes were calculated by following the process shown on the left hand side of the diagram in Fig. 3. To each of the 501 time domain response signals ($y_i(t)$) and the input force signal ($f_j(t)$), white Gaussian noise with a signal to noise ratio (SNR) of 50 dB was added, and the Fourier transform ($\widetilde{Y}_i(\omega)$, $\widetilde{F}_j(\omega)$) calculated. In the frequency domain, alignment error between the input force and measured response was simulated by multiplying the force signal by a cosine error ($\bar{F}_j(\omega) = \widetilde{F}_i(\omega) \cos \beta$), where β is normally distributed with mean 3 and standard deviation of 0.625, based on the data given in Ref. [14]. Then, from the FRFs, curves were fitted between 0 Hz and 1500 Hz and the measured mode shapes (ϕ_{rm}) extracted. The measurement perturbation bound (M_r) was found as the Euclidean norm of the difference between the extracted mode shapes (ϕ_{rm}) and the 'perfect modes' (ϕ_r) from the finite element model. This gave optimum spacings of 0.0481 m, 0.04 m, 0.0282 m, 0.0245 m, and 0.0225 m for the first five modes.

Secondly, the finite difference equation was applied at fifty δ values between 0.001 m and 0.05 m, by following the right hand side of the diagram in Fig. 3. For a particular value of δ, $i = 0.5/\delta + 1$ time domain response signals were extracted from the FD model. Measurement noise, sensor alignment, and curve fitting errors were introduced as above and the measured mode shapes extracted. Then, the finite difference equation was applied and the total error (e_T) calculated as

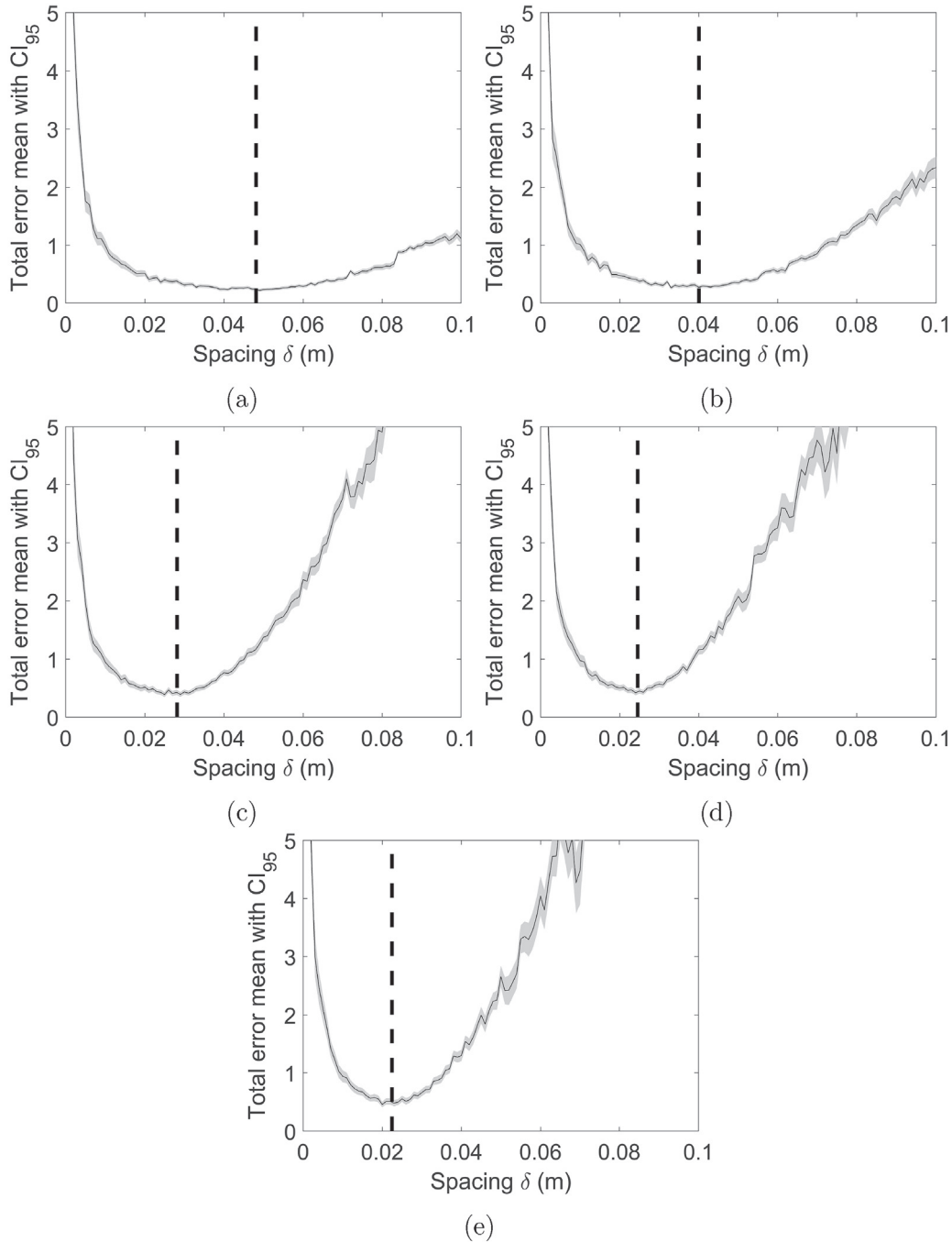$$e_T = \left| \phi_r^{(1)}(x) - D_\delta \phi_{rm}(x) \right| \tag{21}$$

Fig. 4. Results of the numerical validation using a beam with arbitrary boundary conditions for the first 5 bending modes (a)–(e) using the $n = 3$ forward FD equation: Spacing (δ) vs. Total error mean (—) (and 95% confidence interval) as well as predicted optimum spacing δ_{min} (- -).

This was repeated 500 times to give a sufficiently large population of errors for each of the spacings, from which a random sample of 50 was taken and a 95% confidence interval calculated.

3.4. Results and discussion

The results of the numerical validation are presented in Fig. 4a–e for modes 1–5 respectively. In each case, the total error (e_T) mean is shown with its confidence interval. The figures show that by using the δ_{min} value calculated by the optimisation method, the error can be minimised, thus validating the approach. For each mode, values below δ_{min} give rise to much higher

mean errors, showing that the likelihood of the perturbation propagation error will affect the solution rapidly increases as δ shrinks. Contrastingly, as δ becomes larger, the likelihood of the truncation error effecting the solution increases, albeit more gradually than for the propagation error. From this it is sensible to conclude that when δ_{min} is unknown, a larger δ value is more likely to give accurate results. The gradient of the curves increases with wave number, which implies greater sensitivity to the spacing δ. This is to be expected as the $n = 3$ finite difference equation becomes less accurate as the frequency of the wave increases.

Whilst encouraging, this numerical example suffers from two drawbacks. First, the result appears to be restricted to the use of a 3rd order finite difference scheme (Table B.3). Second, the measurement perturbation bound has been assumed to be known perfectly, which is of course impossible in a practical scenario. These issues will be dealt with in Section 4 and 5 respectively.

4. Evaluating other high order derivative norms

Whilst it is advantageous to use the $n = 4k - 1$ forward/backward difference equation, as $\|\phi_r^{(p)}\|$ can be evaluated exactly, it may not always be practically beneficial. In this case, a method to approximate $\|\phi_r^{(p)}\|$ from the standard modal model (ϕ_r, ω_r) must be found. It will now be shown, using the same numerical example as above, that for forward/backward differences with $n = 1$ and $n = 2$ a good approximation to the optimum spacing can be found using the following relationship:

$$\|\phi_r^{(p)}\| \approx \lambda_r^{(p)} \|\phi_r\| \tag{22}$$

which yields optimum spacings approximately given by:

$$\delta_{min}^F \approx \frac{1}{\lambda_r}\left(\frac{4M_r}{\|\phi_r\|}\right)^{(1/2)} \quad \text{and} \quad \delta_{min}^F \approx \frac{1}{\lambda_r}\left(\frac{6M_r}{\|\phi_r\|}\right)^{(1/3)} \tag{23}$$

respectively.

Using the process outlined in Fig. 3 the same numerical investigation was carried out on the structure shown in Fig. 2, this time using the approximate optimum spacings given in Eq. (23). The results for the first and fifth modes for the $n = 1$ and $n = 2$ forward difference equations are presented in Fig. 5a–d respectively.

The results follow the same trends as those of the $n = 3$ forward FD equations presented in section 3, with the propagation error tending to infinity at small spacings, and the numerical error tending to infinity more gradually as δ increases. Most
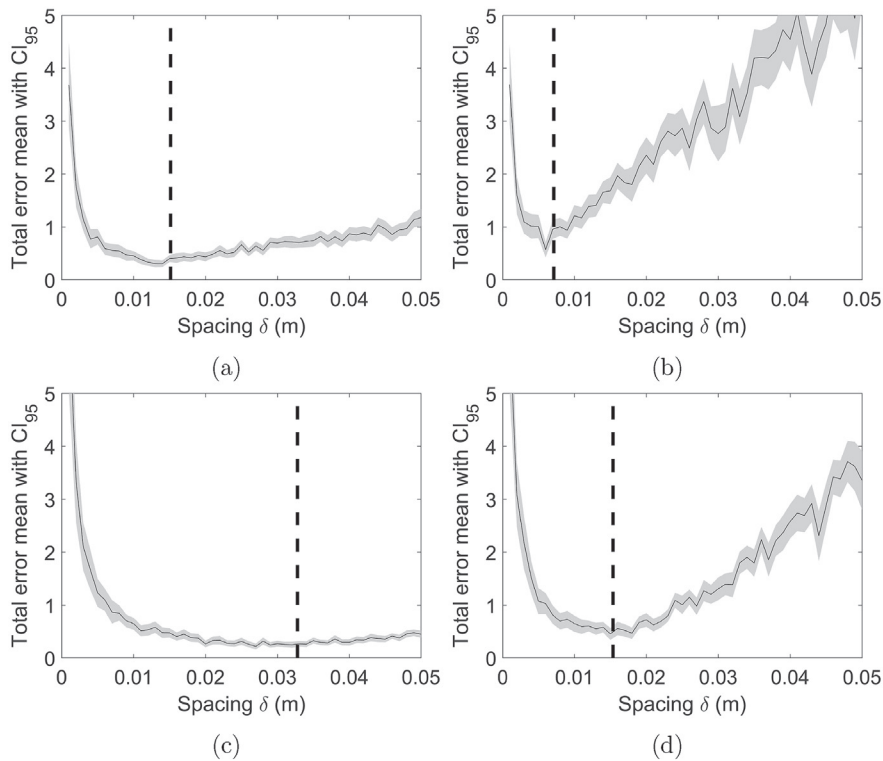

Fig. 5. Results of the numerical validation using a beam with arbitrary boundary conditions: Spacing (δ) vs. Total error mean (—) (and 95% confidence interval) as well as predicted optimum spacing δ_{min} (- -): (a) n = 1 forward difference: Mode 1 (b) n = 1 forward difference: Mode 5 (c) n = 2 forward difference: Mode 1 (d) n = 2 forward difference: Mode 5.

importantly, the approximate optimum spacings still result in the lowest total errors in each case meaning that by using the approximate value for $\|\phi_r^{(p)}\|$ given in Eq. (22) it is possible to optimise the method for any finite difference equation.

5. Approximating the 'perfect modes'

The above examples have assumed perfect knowledge of the measurement perturbation bound M_r, in that the mode shapes ϕ_r could be directly extracted from the finite element model. In practice, this information is unknown and must somehow be approximated. The example from section 3 is now revisited, allowing the high order norm $\|\phi_r^{(p)}\|$ to be calculated explicitly, leaving the only error in approximating the 'perfect modes' ϕ_r.

Assuming that the measurement perturbation $(\overline{\phi}_r)$ at any location x has a random distribution, the mode shapes $\phi_r(x)$ may be approximated as the mean of a set of K measured mode shapes $\{\phi_{rm1}(x), \phi_{rm2}(x), \ldots, \phi_{rmK}(x)\}$, i.e.

$$\phi_r(x) \approx \mu_r(x) = \mu\big(\phi_{rm1}(x), \phi_{rm2}(x), \ldots, \phi_{rmK}(x)\big) \tag{24}$$

where $\mu_r(x)$ is the mean at location x of the rth mode. This approximation should improve as $K \to \infty$.

In order to approximate the bound M_r it is also assumed that the set of measured values $\{\phi_{rm1}(x), \phi_{rm2}(x), \ldots, \phi_{rmK}(x)\}$ is also normally distributed. It is well known that 95% of values from any normally distributed variable lie within the range $\mu \pm 2\sigma$, where σ is the standard deviation. Therefore, considering the measurement perturbation defined in Eq. (7), it can be deduced that approximately 95% of the values of $\overline{\phi}_r$ lie within the following region

$$[\overline{\phi}_r(x)]_{95\%} = [\phi_{rm}(x) - \phi_r(x)]_{95\%} \approx (\mu_r(x) \pm 2\sigma_r(x)) - \mu_r(x) \approx \pm 2\sigma_r(x) \tag{25}$$

Substituting this into the measurement perturbation bound defined in Eq. (9) an approximation on M_r can be found:

$$\|2\sigma_r\| \leq M_r \tag{26}$$

The accuracy of which should improve with the number of measurements K.

Before discussing the effect of this approximation on δ_{min}, the assumptions made above are discussed. It is a perfectly valid assumption that measurement error such as noise will be randomly distributed; however, errors such as curve fitting (especially
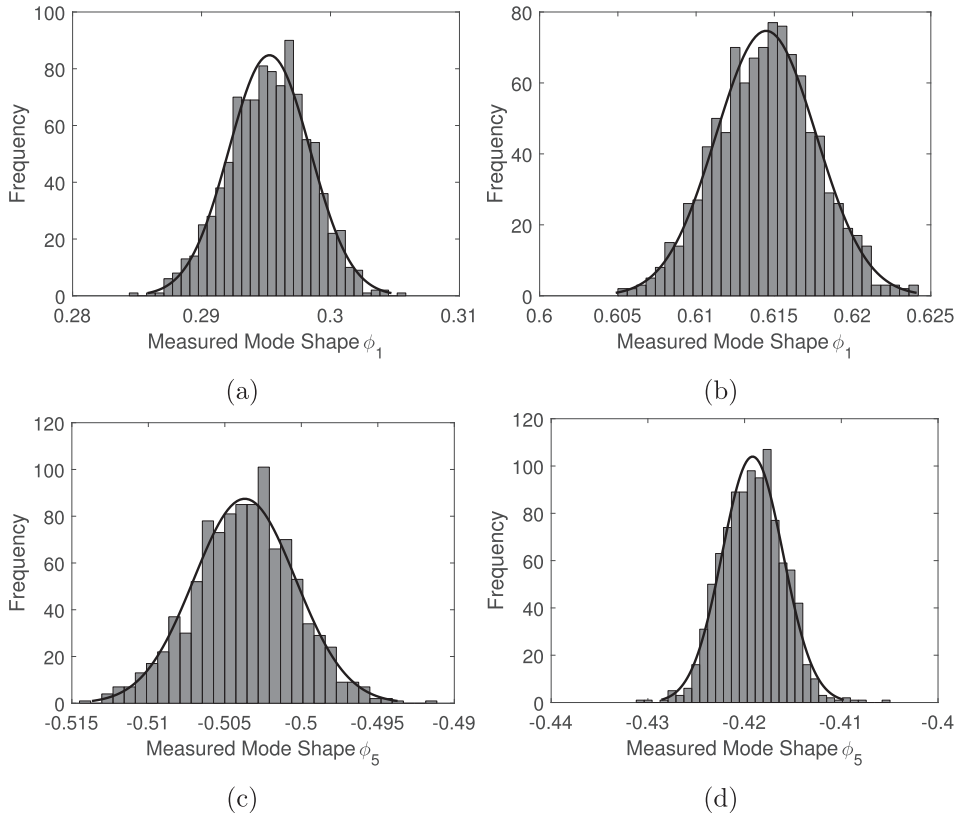

Fig. 6. Histograms of 1000 measured mode shapes ($\overline{\phi}_r$) with normal density function: (a) Mode 1 at location $x = 0$ m with $\mu_1(x = 0) = 0.2953$ and $\sigma_1(x = 0) = 0.032$ (b) Mode 1 at location $x = 0.25$ m with $\mu_1(x = 0.25) = 0.6146$ and $\sigma_1(x = 0.25) = 0.032$ (c) Mode 5 at location $x = 0$ m with $\mu_5(x = 0) = -0.5037$ and $\sigma_5(x = 0) = 0.031$ (d) Mode 5 at location $x = 0.25$ m with $\mu_5(x = 0.25) = -0.4195$ and $\sigma_5(x = 0.25) = 0.033$.
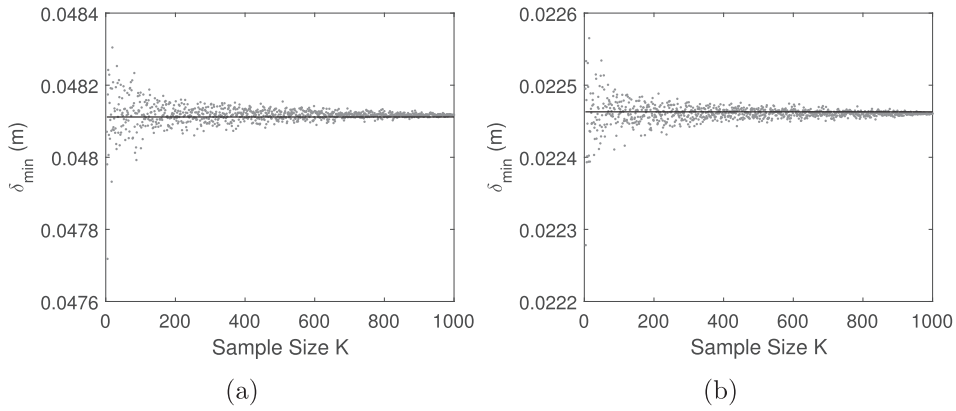
Fig. 7. The effect of sample size (or number of measurement repetitions) on δ_{min} prediction for mode 1 (a) and mode 5 (b).
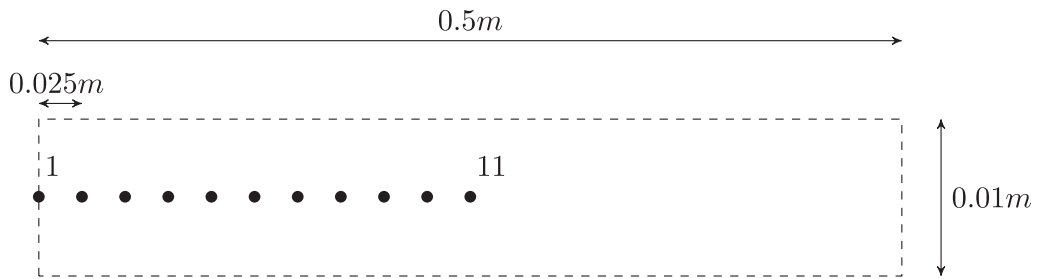

Fig. 8. A free-free beam of length 0.5 m, diameter 0.01 m, with 11 equally spaced measurement locations, used for experimental validation of error analysis.

if the process is automated) may be more systematic in nature and will effect the accuracy of this approximation. The validity of the second assumption, that a set of measured mode shapes at any location x is normally distributed, is now demonstrated using the example given in section 3. To the finite element mode shapes ϕ_r noise, misalignment, and curve fitting errors were introduced as before. This was then repeated 1000 times to represent $K = 1000$ experimental repetitions. The data sets at $x = 0$ m and $x = 0.25$ m were extracted and individual histograms generated. The results for modes 1 and 5 are plotted in Fig. 6, along with the normal density function generated using the associated μ and σ. The figures demonstrate that independent of wave number or measurement location, the measured data sets all have a (roughly) normal distribution, thus validating the assumption made above.

The impracticality of repeating an experiment 1000 times would obviously render the method worthless; therefore, the above approximation must now be validated for small values of K. Consequently, the numerical investigation from section 3 was repeated, yielding δ_{min} values of 0.0481 m and 0.0225 m for the first and fifth bending modes respectively.
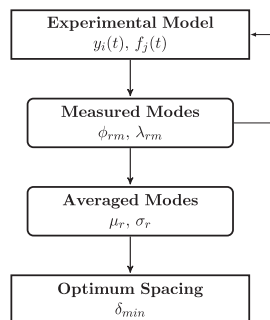

Fig. 9. Flow chart detailing the experimental process for calculation of optimum spacings.
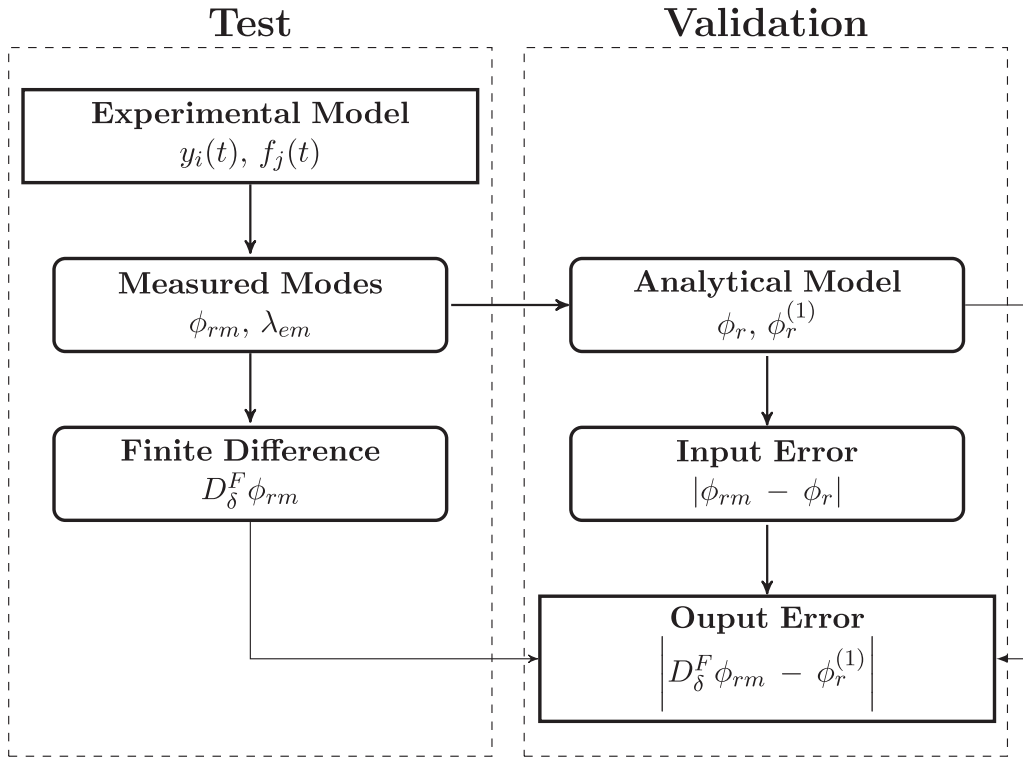
Fig. 10. Flow chart detailing the process used to experimentally validate error analysis.

Additionally, from the 1000 sets of measured modes, a random sample of size $K = 3$ were extracted. Using this sample δ_{min} was calculated for the first and fifth bending modes ($r = 1, 5$) using the following result:

$$\delta_{min}^F = \frac{1}{\lambda_r}\left(\frac{80\|2\sigma_r\|}{9\|\mu_r\|}\right)^{\left(\frac{1}{4}\right)} \tag{27}$$

This process was then repeated for sample sizes between $K = 3$ and $K = 1000$. The approximate δ_{min} values are plotted against the expected values (0.0481 m, and 0.0225 m) in Fig. 7. The figures clearly show that increasing the sample size (i.e. the number of measurement repetitions) increases the accuracy of the approximation as expected. In both cases, the data tends to a value at or near the expected δ_{min} value. However, even with very small sample sizes of $K = 3$, the prediction is accurate to within 0.62% for mode 1 and 0.81% for mode 5; thus, yielding inaccuracies of just +0.14 mm and −0.39 mm respectively. Due to the accuracy in these approximations the optimum spacings given in Eqs. (13) and (14) are redefined such that:

$$\delta_{min}^F \approx \frac{1}{\lambda_r}\left(\frac{\|2\sigma_r\|}{\|\mu_r\|}\sum_{k=0}^{n}\frac{|a_k|}{nT}\right)^{\frac{1}{n+1}}$$

$$\delta_{min}^C \approx \frac{1}{\lambda_r}\left(\frac{\|2\sigma_r\|}{\|\mu_r\|}\sum_{k=-n}^{n}\frac{|a_k|}{2nT}\right)^{\frac{1}{2n+1}} \tag{28}$$

where $\lambda_r \approx \mu(\lambda_{rm})$.

This section has concentrated on approximating the 'perfect modes' from a measured data set, showing that by obtaining a very small number of mode shape measurements, it is possible to accurately calculate the optimum spacing. Thus far, the effect of approximating the high order measurement norm ($\|\phi_r^{(p)}\|$), and the effect of approximating the 'perfect' mode shapes (ϕ_r) have been discussed in isolation, using numerical examples. The next section, looks to utilise an experimental data set to combine both approximations, and validate the effectiveness of the optimised finite difference method in practice.

6. Experimental investigation

This section experimentally validates the error analysis, utilising data from a free-free beam to demonstrate how effective the optimum spacings can be in practice. The 'perfect modes' are approximated from three repetitions (i.e. $K = 3$), and the $N = 1$

finite difference scheme is used to include the effect of approximating the high order norm. A free-free beam was chosen as an example since the boundary conditions can be easily reproduced under test conditions; therefore, the finite difference results can be compared with the analytical solutions to the beam equation.

6.1. Experimental calculation of optimum spacings

A cylindrical beam of length 0.5 m and diameter 0.02 m was suspended at each end using light strings to produce the free-free boundary conditions. The beam had standard steel material properties (density ρ = 7750 kg m^{-3}, Young's Modulus E = 200 GPa) and standard geometry (cross section A = 3.14 × 10^{-4} m^2, area moment of inertia I = 7.9 × 10^{-9} m^4). The response was measured with a single accelerometer at 11 equally spaced locations ($\{x_1, x_2, \ldots, x_{11}\}$) separated by 0.025 m, by striking the beam at location 1 with an impulse hammer, as shown in Fig. 8.

In order to calculate the optimum spacing using only experimental data the process depicted in Fig. 9 was followed. An experimental modal analysis was carried out on the data set to extract the measured mode shapes (ϕ_{rm}) and natural frequencies (ω_{rm}), from which the eigenvalues were calculated as

$$\lambda_{rm}^4 = \frac{\rho A \omega_{rm}^2}{EI} \tag{29}$$

considering only the first five bending modes. This was repeated three times, always replacing the accelerometer so as to include location error in the data, resulting in three modal models. The optimum spacings for the n = 1 FD equation were then calculated from the three repetitions, using the following result:

$$\delta_{min}^F \approx \frac{1}{\lambda_r} \sqrt{\frac{4\|2\sigma_r\|}{\|\mu_r\|}} \tag{30}$$

giving δ_{min} values of 0.038 m, 0.055 m, 0.056 m, 0.032 m, 0.033 m for the first five modes respectively.

Placing an accelerometer at a location correct to the nearest 0.001 m is difficult in practice, and seeing as the accelerometer has a width of 0.005 m, the five optimum spacings were averaged, and a value of 0.04 m used as the optimum spacing for all five modes.

6.2. Experimental validation

The experimental data set included measurements at the eleven locations of interest $\{x_1, x_2, \ldots, x_{11}\}$ as well as eleven finite difference locations $\{x_1 + 0.04 \text{ m}, x_2 + 0.04 \text{ m}, \ldots, x_{11} + 0.04 \text{ m}\}$. The following process (outlined in Fig. 10) was performed for validation purposes only, and would usually be unnecessary.

From the data set of twenty-two response signals, the measured mode shapes and eigenvalues were extracted, the FD equation applied to the mode shapes to obtain $D_\delta^F \phi_{rm}$, and the eigenvalues were used with the solution to the beam equation to
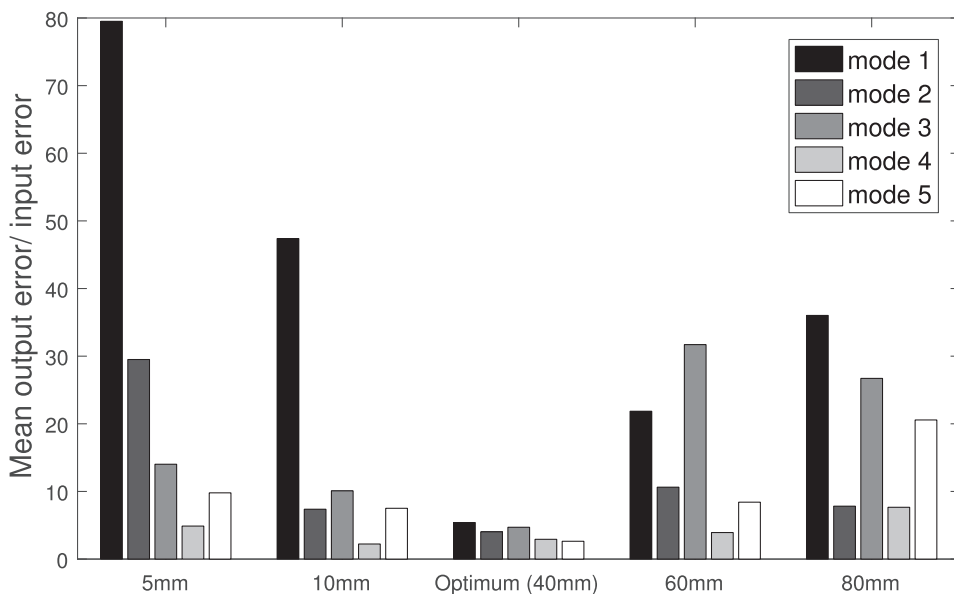

Fig. 11. Bar chart comparing errors from experimental validation of error analysis at five spacings.

construct an analytical model (ϕ_r, and $\phi_r^{(1)}$). The input error to the finite difference equation was calculated as the difference between the measured and analytical modes, whilst the output error was taken as the difference between $D_\delta^F \phi_{rm}$ and the analytical rotational modes ($\phi_r^{(1)}$).

In this context, the aim is therefore to minimise the output error, compared to the input error, by adjusting the measurement spacing δ. To compare the optimum spacing with other arbitrary spacings, the process was repeated at four other spacings, 0.005 m, 0.01 m, 0.06 m, and 0.1 m, each time calculating both the input and output errors.

6.3. Results and discussion

The results of the experimental validation are presented in Fig. 11, which shows the ratio of the output error to the input error averaged over the eleven locations, for each of the five spacing values. It can be seen that the optimum spacing (or a value
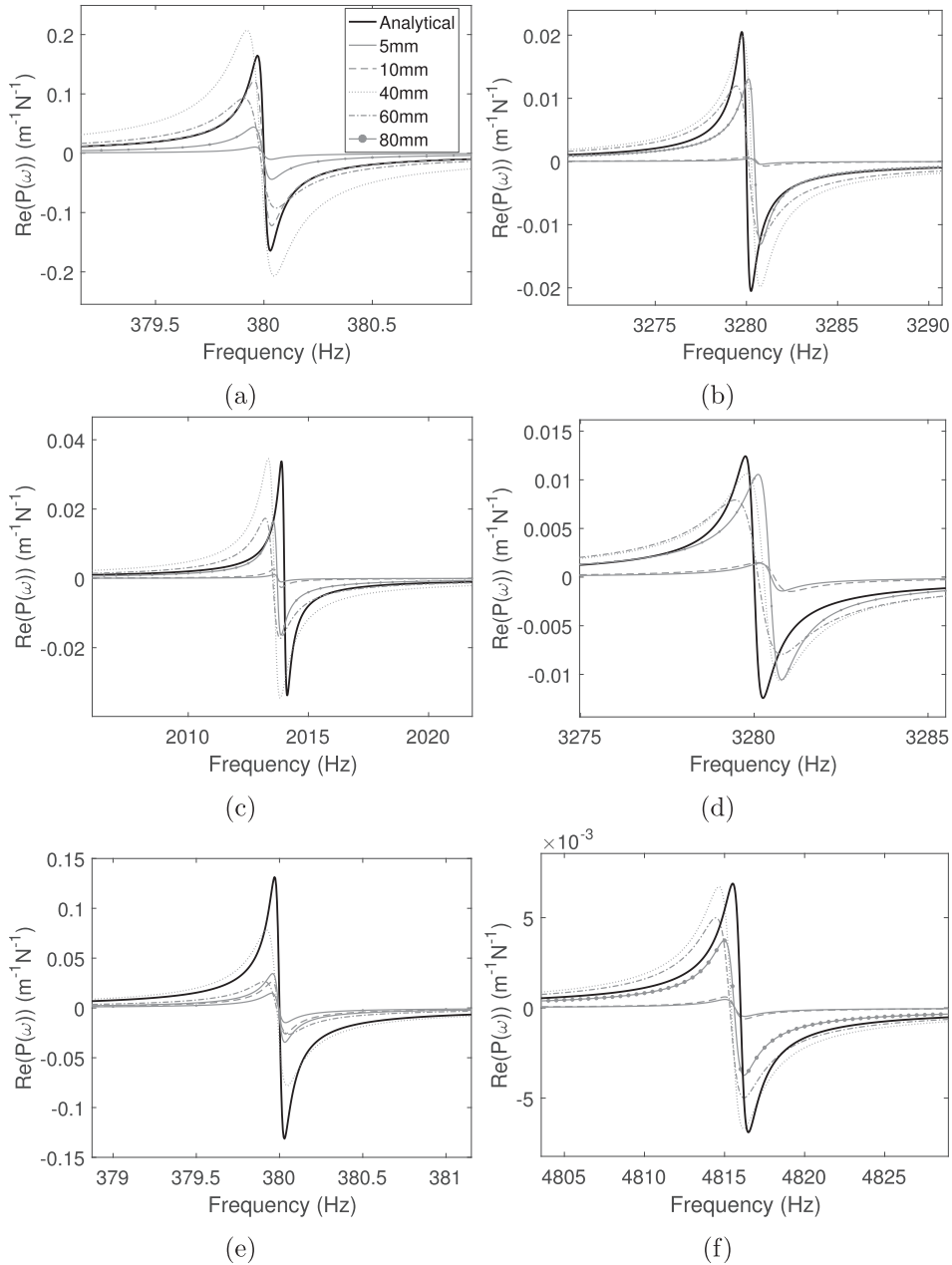

Fig. 12. Frequency Response Function plots comparing the real part of the rotation/moment FRF $P_{ij}(\omega)$ for both analytical and experimental models: (a) location 1, mode 1 (b) location 1, mode 4 (c) location 6, mode 3 (d) location 6, mode 4 (e) location 11, mode 1 (f) location 11, mode 5.

close to it) can significantly reduce the error of the finite difference method with non-exact data.

Of all the results plotted in Fig. 11, there is only one scenario (Mode 4, 0.01 m spacing) where the performance was better than that for the optimum spacing. This may be because the correct spacing for this mode was actually calculated to be 0.032 m, or it is also possible that, due to statistical variation in the data, the error for this mode in the 0.01 m spacing experiment was significantly lower than in the others.

Using the calculated rotational mode shapes, for each of the five spacings, the rotational displacement/excitation moment FRF, $P_{ij}(\omega)$ (as given in Eq. (2)), was calculated. These experimental FRFs are compared with that of the analytical model in Fig. 12, where six individual modes at three measurement locations across the length of the beam are presented. In each case, the optimum spacing (40 mm) results in a significantly more accurate result, with the exception of mode 1 at location 1 (Fig. 12a), where 10 mm spacing produced a highly accurate result. However, Fig. 12 also demonstrates the significant variability in the results when using a nonoptimal spacing, as only 40 mm spacing produces repeatedly accurate results.

7. Conclusion

In structural dynamics, the measurement of rotational degrees-of-freedom has not evolved to the same extent as translational measurements, despite the need for rotational information in many engineering applications. It is, however, possible to synthesise the rotational information from translational data, using numerical methods such as finite differences. Whilst the application of such methods is seemingly simple, they are limited by the user's choice of spacing. Reducing the spacing between data points will, naturally, reduce the numerical error associated with the finite difference equation; however, the method also becomes unstable when the spacing is reduced, as small perturbations in the input data propagate through the method causing large errors in the output data.

In the present study, an analytical error analysis has been presented to prove the instability of the finite difference method when using non-exact data. Then, a new optimum spacing, which balances the numerical and propagation errors, has been proposed. The method uses the general form of the beam equation and its higher order derivative norms, but does not require any analytical parameters and requires only that the structure exhibits beam-like dynamic behaviour. The method is exact for finite difference equations of the order $n = 4k - 1$, where the derivative norm can be evaluated exactly. For other finite difference equations, it has been observed that a good approximation can still be found. The method also requires knowledge of the measurement error for the experimental mode shapes. It has been shown that in practice this measurement error can be easily approximated by performing just three repeat measurements of the translational mode shapes. Consequently, the method is straightforward to implement in practice and has minimal additional experimental or computation cost compared to a naive approach.

Results from a numerical investigation on a beam with arbitrary boundary conditions have been used to validate the error analysis and demonstrate the effectiveness of the derivative approximations. An experimental study has also been performed to demonstrate how the optimised finite difference method may be used in practice. A comparison of errors, at optimal and non-optimal spacings, shows that the presented method can significantly reduce the error when using the finite difference method with non-exact data.

Acknowledgements

Appendix A. Finite difference derivation

Using Taylor's theorem it is possible to derive a bound on the truncation error of the finite difference equation given in Eq. (3). The theorem states that if a real valued function $\phi_r(x)$ is differentiable at point x, then a linear approximation to the function at point $x + \delta$, where δ is a real positive constant, can be found as:

$$\phi_r(x + \delta) = \phi_r(x) + \delta\phi_r^{(1)}(x) + \frac{\delta^2}{2}\phi_r^{(2)}(x) + \cdots \qquad (A.1)$$

Eq. (A.1) can be rearranged to give an approximation of the first derivative at point x ($\phi_r^{(1)}(x)$):

$$\phi_r^{(1)}(x) = \frac{\phi_r(x + \delta) - \phi_r(x)}{\delta} - \frac{\delta}{2}\phi_r^{(2)}(x) + \cdots \qquad (A.2)$$

resulting in the well known first order forward finite difference equation. Substituting for the forward finite difference operator D_δ^F we have that

$$\phi_r^{(1)}(x) = D_\delta^F\phi_r(x) - \frac{\delta}{2}\phi_r^{(2)}(x) + \cdots \qquad (A.3)$$

Rearranging and taking the absolute value, the error associated with the finite difference approximation is found from the first truncation term in the Taylor series

$$\left| \phi_r^{(1)}(x) - D_\delta^F \phi_r(x) \right| = \left| \frac{\delta}{2} \phi_r^{(2)}(x) + \cdots \right| \tag{A.4}$$

Using the well known subadditivity property of the absolute value ($|a + b| \leq |a| + |b|$) it is found that

$$\left| \phi_r^{(1)}(x) - D_\delta^F \phi_r(x) \right| \leq \frac{\delta}{2} \left| \phi_r^{(2)}(x) \right| + \cdots \tag{A.5}$$

Since the value of $\phi_r^{(2)}(x)$ is unknown, a bound on the error can be found by taking the Euclidean norm of the function $\phi_r^{(2)}$.

$$\left| \phi_r^{(1)}(x) - D_\delta^F \phi_r(x) \right| \leq \frac{\delta}{2} \| \phi_r^{(2)} \| \tag{A.6}$$

where $\| \phi_r^{(2)} \|$ is the Euclidean norm of the vector $\phi_r^{(2)}$.

Appendix B. Tables

Table B.1
Finite difference formulae with coefficients for optimisation for $n = 1$ points.

n = 1	Formula	Accuracy	$\sum |a_k|$	T
Backward	$\frac{\phi(x) - \phi(x - \delta)}{\delta}$	$O(\delta)$	2	1/2
Forward	$\frac{\phi(x + \delta) - \phi(x)}{\delta}$	$O(\delta)$	2	1/2
Central	$\frac{\phi(x + \delta) - \phi(x - \delta)}{2\delta}$	$O(\delta^2)$	1	1/6

Table B.2
Finite difference formulae with coefficients for optimisation for $n = 2$ points.

n = 2	Formula	Accuracy	$\sum |a_k|$	T
Backward	$\frac{3\phi(x) - 4\phi(x - \delta) + \phi(x - 2\delta)}{2\delta}$	$O(\delta^2)$	4	1/3
Forward	$\frac{-3\phi(x) + 4\phi(x + \delta) - \phi(x + 2\delta)}{2\delta}$	$O(\delta^2)$	4	1/3
Central	$\frac{-\phi(x + 2\delta) + 8\phi(x + \delta) - 8\phi(x - \delta) + \phi(x - 2\delta)}{12\delta}$	$O(\delta^4)$	3/2	1/30

Table B.3
Finite difference formulae with coefficients for optimisation for $n = 3$ points.

n = 3	Formula	Accuracy	$\sum |a_k|$	T
Backward	$\frac{11\phi(x) - 18\phi(x - \delta) + 9\phi(x - 2\delta) - 2\phi(x - 3\delta)}{6\delta}$	$O(\delta^3)$	20/3	1/4
Forward	$\frac{-11\phi(x) + 18\phi(x + \delta) - 9\phi(x + 2\delta) + 2\phi(x + 3\delta)}{6\delta}$	$O(\delta^3)$	20/3	1/4
Central	$(\star)$	$O(\delta^6)$	5/3	1/150

$$(\star) \frac{\phi(x + 3\delta) - 9\phi(x + 2\delta) + 45\phi(x + \delta) - 45\phi(x - \delta) + 9\phi(x - 2\delta) - \phi(x - 3\delta)}{60\delta}$$

References

[1] T. Schmitz, R. Donalson, Predicting high-speed machining dynamics by substructure analysis, CIRP Ann. - Manuf. Technol. 49 (1) (2000) 303–308.
[2] T.L. Schmitz, G.S. Duncan, Three-component receptance coupling substructure analysis for tool point dynamics prediction, J. Manuf. Sci. Eng. 127 (4) (2005) 781–790.
[3] A. Moorhouse, A. Elliott, T. Evans, In situ measurement of the blocked force of structure-borne sound sources, J. Sound Vib. 325 (4) (2009) 679–685.
[4] P. Varoto, M. Lofrano, T. Cicogna, L. Oliveira, K. McConnell, Moment mobility frf measurement techniques, in: Proceedings of the Twentyfourth International Modal Analysis Conference, 2006.
[5] D. de Klerk, D.J. Rixen, S. Voormeeren, General framework for dynamic substructuring: history, review and classification of techniques, AIAA J. 46 (5) (2008) 1169–1181.
[6] S.S. Sattinger, A method for experimentally determining rotational mobilities, J. Acoust. Soc. Am. 64 (6) (1978) 1734–1764.
[7] A. Sestieri, P. Salvini, W. D'Ambrogio, Reducing scatter from derived rotational data to determine the frequency response function of connected structures, Mech. Syst. Signal Process. 5 (1) (1991) 25–44.
[8] M.L.M. Duarte, D.J. Ewins, Some insights into the importance of rotational degrees-of-freedom and residual terms in coupled structure analysis, in: Proceedings of the Thirteenth International Modal Analysis Conference, 1995.
[9] M.L.M. Duarte, D.J. Ewins, Rotational degrees of freedom for structural coupling analysis via finite-difference technique with residual compensation, Mech. Syst. Signal Process. 14 (2) (2000) 205–227.
[10] A. Elliott, A.T. Moorhouse, Characterisation of structure borne sound sources from measurement in-situ, J. Acoust. Soc. Am. 123 (5) (2008) 3176.
[11] A. Elliott, A. Moorhouse, G. Pavić, Moment excitation and the measurement of moment mobilities, J. Sound Vib. 331 (11) (2012) 2499–2519.
[12] J. Stewart, Calculus: Early Transcendentals, Cengage Learning, 2015.
[13] S. Lu, S. Pereverzev, Regularization Theory for Ill-posed Problems: Selected Topics, De Gruyter, 2013.
[14] H.S. Kim, T.L. Schmitz, Bivariate uncertainty analysis for impact testing, Meas. Sci. Technol. 18 (11) (2007) 3565–3571.